Electronic and Geometric Stabilities of Clusters with Transition Metal Encapsulated by Silicon

Kiichirou Koyasu,[†] Junko Atobe,[†] Minoru Akutsu,[†] Masaaki Mitsui,[†] and Atsushi Nakajima*[,†,‡]

Department of Chemistry, Faculty of Science and Technology, Keio University, 3-14-1 Hiyoshi, Kohoku-ku, Yokohama 223-8522, Japan, and CREST, Japan Science and Technology Agency (JST), c/o Department of Chemistry, Keio University, Yokohama 223-8522, Japan

Received: October 14, 2006; In Final Form: October 19, 2006

Silicon clusters mixed with a transition metal atom, MSi_n, were generated by a double-laser vaporization method, and the electronic and geometric stabilities for the resulting clusters with transition metal encapsulated by silicon were examined experimentally. By means of a systematic doping with transition metal atoms of groups 3, 4, and 5 (M = Sc, Y, Lu, Ti, Zr, Hf, V, Nb, and Ta), followed by changes of charge states, we explored the use of an electronic closing of a silicon caged cluster and variations in its cavity size to facilitate metal-atom encapsulation. Results obtained by mass spectrometry, anion photoelectron spectroscopy, and adsorption reactivity toward H_2O show that the neutral cluster doped with a group 4 atom features an electronic and a geometric closing at $n = 16$. The MSi_{16} cluster with a group 4 atom undergoes an electronic change in (i) the number of valence electrons when the metal atom is substituted by the neighboring metals with a group 3 or 5 atom and in (ii) atomic radii with the substitution of the same group elements of Zr and Hf. The reactivity of a halogen atom with the MSi_{16} clusters reveals that $VSi_{16}F$ forms a superatom complex with ionic bonding.

1. Introduction

The magic-number behavior of Na_n clusters and its explanation based on the electron shell model[1] has stimulated experimental and theoretical studies[2,3] searching for magic clusters by varying the sizes, compositions, and charges for other chemical species. Recent examples include fullerenes and metallofullerenes,[4,5] metallocarbohedrenes,[6] gold-related compounds,[7,8] sodium-lead binary compounds,[9] and organometallic sandwich compounds.[10]

Since the discovery of C_{60},[4] many attempts have been made to assemble nanostructured materials from these finite-sized stable clusters. The fabrication of cluster-assembled materials is dependent upon finding a suitable building block for a cluster that is chemically stable and that interacts weakly with other clusters of the same material. To ensure the chemical stability of a cluster, it is crucial to produce a closed electron configuration with a large energy gap between the highest occupied molecular orbital (HOMO) and the lowest unoccupied molecular orbital (LUMO). Indeed, the large HOMO−LUMO gap of C_{60} is responsible for its chemical inertness and its ability to assemble into molecular crystals, as well as its high symmetry.[4]

Silicon is undoubtedly an important material in electronic devices, and silicon clusters have also attracted great attention as building blocks for silicon-based nanomaterials. However, pure silicon clusters are unsuitable as building blocks; no pure Si_n clusters form the fullerene-like cage structure by themselves[11] because their dangling bonds make them chemically reactive.[12−17] These results are ascribed to the fact that silicon atoms much prefer sp^3 hybridization to sp^2. In contrast, carbon atoms can appear with sp, sp^2, or sp^3 hybridization in compounds.

Since the dangling bonds makes Si clusters unstable, especially when they aggregate themselves, it is very important to quench that bond to make cluster-assembled materials.[18−19] One of the strategies for doing so is the doping of a suitable metal atom into a pure Si cluster; a highly stabilized cluster will open up a new avenue to cluster-assembled materials made from Si atoms. With metal atom doping, closed-shell electronic structures might lead to species that are remarkably stable, such as a new class of clusters with transition metal encapsulated by silicon. Since Beck[20] described the remarkable formation of MSi_{15}^+ and MSi_{16}^+ (M = Cr, Mo, W), many stable MSi_n (at $n = 12$, 14, and 16, etc) species have been reported in which various factors accounting for their formation have been examined experimentally[18,20] and theoretically.[19] These factors include the electronic stability of the octet (18 electron) rule[19i] or the geometric stability of a metal-encapsulated structure.[19a−d] Depending on the kind of metal atom, even a single one may significantly affect the structure of a silicon cluster, bringing about magic-number behavior in the mass spectrometry of MSi_n. A "magic" cluster, in which metal is encapsulated in a Si cage, can be viewed as a superatom,[21] and it is therefore of much interest to verify experimentally this "superatom" behavior in clusters with transition metal encapsulated by silicon. The existence of superatoms suggests that, with proper assembly, it should be possible to develop silicon-based devices for various optoelectronic applications.[19b]

Toward this challenging end, efforts to examine the superatom behavior involved in electronic and geometric shell closings have focused on substituting the central atom in a Si cage, and we have presented experimental evidence for a highly stable cluster corresponding to $M@Si_{16}$ (M = Sc, Ti, and V).[18d] In

* To whom correspondence should be addressed. E-mail: nakajima@chem.keio.ac.jp.
[†] Keio University.
[‡] Japan Science and Technology Agency.

10.1021/jp066757f CCC: $37.00
Published on Web 12/14/2006

the present article, we would like to present a full account of our experimental results obtained for the electronic and geometrical structures of MSi_n clusters, which have been intensively studied by systematically changing metal atoms among the atoms of groups 3, 4, and 5 (M = Sc, Y, Lu, Ti, Zr, Hf, V, Nb, and Ta). The techniques used were mass spectrometry and anion photoelectron spectroscopy (PES), the latter being especially useful for a quantitative understanding of the electronic properties of neutral clusters. An improved ability to produce cold mixed clusters enabled us to selectively aggregate MSi_{16} clusters and to obtain more detailed electronic structure information. The change in total valence electrons upon the substitution of a group 3 or group 5 element for a group 4 element altered the magic-number behavior and instead produced charged mixed clusters; surprisingly, anionic $ScSi_{16}^-$ and cationic VSi_{16}^+, $NbSi_{16}^+$, and $TaSi_{16}^+$ were generated, as well as neutral $TiSi_{16}$. The $TiSi_{16}$ cluster exhibited a large HOMO−LUMO gap of around 1.9 eV, and with halogen atom doping permitted definitive PES peak assignments. This result suggests the possibility of producing an ionically bound superatom complex of $VSi_{16}^+F^-$. Finally, the paper presents experimental evidence for the geometric criterion which must be fulfilled if a metal atom is to be encapsulated inside a Si_{16} cage.

2. Experimental Section

Details of the experimental setups for chemical adsorption and photoelectron spectroscopy have been described extensively elsewhere.[18c] Briefly, cations/neutrals/anions of silicon clusters doped with one metal atom (MSi_n: M = Sc, Y, Lu, Ti, Zr, Hf, V, Nb, and Ta) were generated by a combination of the dual-laser vaporization method and the molecular beam method. Both the Si and the pure metal rods were independently vaporized by means of two frequency-doubled Nd^{3+}:YAG lasers. Very intense supersonic helium gas pulses were employed to recombine and cool the laser-produced metal vapors. A high-pressure Even-Lavie pulsed valve (10 Hz) was used at a stagnation pressure of 100 atm,[22] which was suitable for the effective formation of MSi_n. The optimum laser fluence required to maximize the cluster intensities varied according to the properties of the metal under investigation. Here, the Si rod was located upstream, while the metal rod was located downstream. An exchange of the rod positions resulted in less mixing of the two components in the mass distribution of the binary clusters.

A mass analysis of the neutral clusters ionized by an F_2 laser (157 nm, 7.90 eV) and of the charged clusters was performed with time-of-flight mass spectrometry. The laser power dependence for the photoionization had been measured to establish the conditions for one-photon ionization of the MSi_n clusters by changing the flow rate of He gas toward the laser path tubing between the laser exit and a CaF_2 chamber window. The laser fluence typically used was below 1 mJ/cm^2, where a linear dependence of ion intensity against laser power was obtained.

To obtain information on the geometric structure of the binary clusters, the adsorption reactivity of the clusters was measured by means of a flow-tube reactor (FTR)[23] combined with the cluster source. Water vapor diluted with 1.5 atm of He gas was used as the reactant gas and was injected into the FTR. The binary clusters were synchronously mixed with the reactant gas pulse at FTR and reacted with the reactant molecule. The products of the clusters were mass-analyzed by the TOF mass spectrometer, and the mass spectra of the clusters were measured before and after the reaction so that the relative adsorption reactivity might be measured.

In the photoelectron spectroscopy measurements of the mixed cluster anions, the clusters were accelerated to 900 eV. After the ions were mass-selected, a pulsed electric decelerator considerably reduced their kinetic energy before they entered the photodetachment region of a magnetic-bottle-type electron spectrometer. Then, we focused the fifth harmonic (213 nm, 5.83 eV) of a pulsed Nd^{3+}:YAG laser onto the mass-selected clusters to detach photoelectrons. The electrons were guided by a strong, inhomogeneous magnetic field, and subsequently with a weak guiding magnetic field, and detected by a microchannel plate (MCP). Their kinetic energy was analyzed by their TOF and calibrated by the transition of Au^- ($^2S_{1/2} \leftarrow {}^1S_0$).[24,25] The photoelectron signal was typically accumulated over 20000−40000 laser shots.

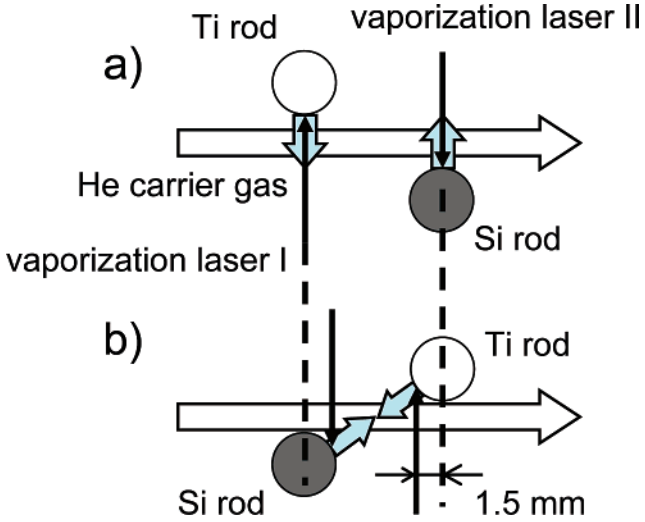

Figure 1. Schematic diagrams of (a) the previous cluster source and (b) the modified "face-to-face" cluster source. The solid circle (●) and open circle (○) represent a Si and a transition metal rod, respectively. In (a), the two rods were laser-vaporized with a delay of about 5 μs synchronized with the He carrier gas speed. In (b), on the other hand, the focusing positions were shifted (1.5 mm) and off the front of the sample rods to be opposite each other, and the two vaporization lasers were simultaneously irradiated within 300−500 ns.

Modification of a Cluster Source. The cluster source was modified so that the MSi_n clusters could be more effectively generated. Figure 1 shows the schematic diagrams of (a) the original cluster source and (b) the modified "face-to-face" cluster source. In the previous source, two sample rods were laterally separated by 4 mm from each other, and their front surfaces were vaporized independently by the following steps: (1) One sample rod was first laser-vaporized; (2) the generated vapor was carried downstream with the He carrier gas; (3) the other sample rod was laser-vaporized when the vapor of the first component arrived; and (4) the two vapors were mixed. Then, the two rods were laser-vaporized with a delay of about 5 μs in synchronization with the He carrier gas speed. While the vapor of the first element vaporized was carried to the locations of the second target, it cooled and formed aggregates of itself. Hence, both individual clusters, which consisted of one element and mixed clusters, were generated, and so we deduced that this cooling process significantly lowers the formation efficiency of a binary mixed cluster.

At that point, the focusing positions of the vaporization lasers were modified and were shifted toward each other by 1.5 mm and moved off the front of the sample rods (Figure 1b). This shift of the focusing positions facilitated the vaporization of the curved surface of the sample rods and the effective mixing of the hot sample plasmas. The improvements occurred because the atoms and ions in the plasma undergo a highly directional expansion perpendicular to the target surface.[26] In fact, the mixed

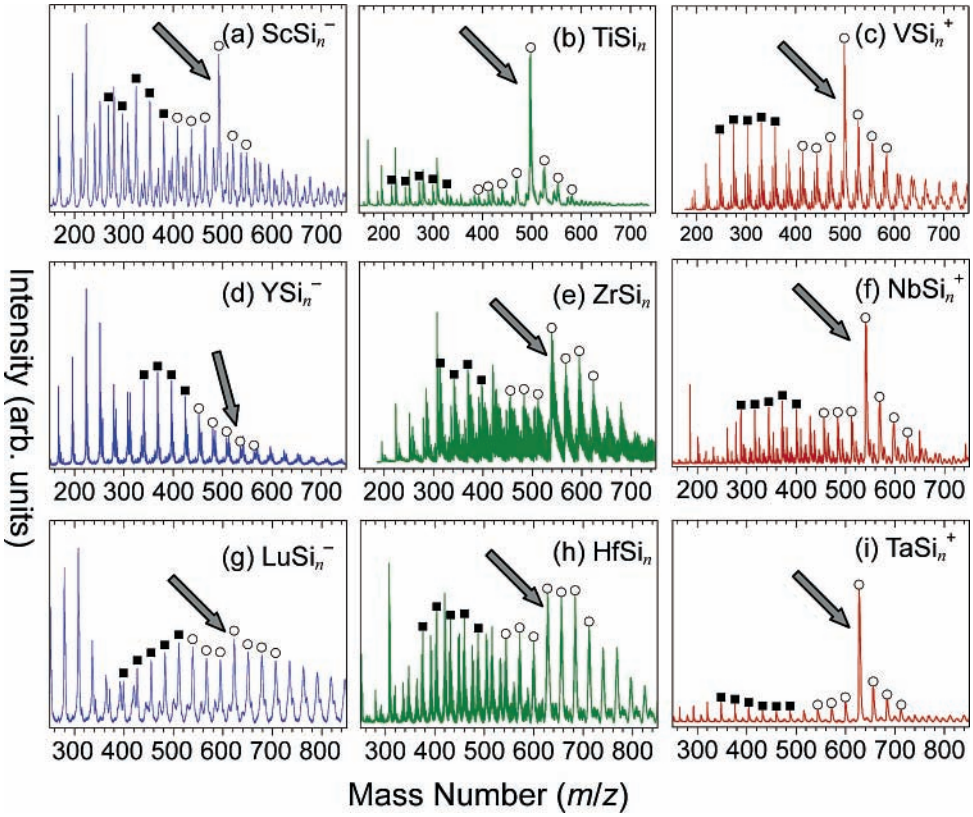

Figure 2. Mass spectra of metal atom doped Si_n clusters (MSi_n): (a) $ScSi_n^-$, (b) $TiSi_n$, (c) VSi_n^+, (d) YSi_n^-, (e) $ZrSi_n$, (f) $NbSi_n^+$, (g) $LuSi_n^-$, (h) $HfSi_n$, and (i) $TaSi_n^+$. Left three columns are anionic MSi_n^- (M = Sc, Y, and Lu), middle three columns are neutral MSi_n (M = Ti, Zr, and Hf), and right three columns are cationic MSi_n^+ (M = V, Nb, and Ta). Bimodal distributions were typically observed. The solid square (■) and open circle (○) represent the two distributions (I and II). Distribution I was similar to that of pure Si_n in their charge state, while distribution II had a prominent peak at MSi_{16}, indicating that species with 20 (68) valence electrons in total are particularly stable. Arrows indicate the mass peaks of the $MSi_{16}^{+/0/-}$ clusters.

clusters were produced efficiently when the two rods were almost simultaneously vaporized, within a few hundreds nanoseconds (ns). This modification resulted in the effective formation of binary M−Si clusters.

3. Results and Discussion

3.1. Mass Distribution of M−Si Composite Clusters.

Figure 2 shows typical mass spectra of the metal atom doped Si_n clusters ($MSi_n^{-/0/+}$): (a) $ScSi_n^-$, (b) $TiSi_n$, (c) VSi_n^+, (d) YSi_n^-, (e) $ZrSi_n$, (f) $NbSi_n^+$, (g) $LuSi_n^-$, (h) $HfSi_n$, and (i) $TaSi_n^+$. Here, the neutral clusters of $TiSi_n$, $ZrSi_n$, and $HfSi_n$ were photoionized by a pulsed F_2 laser (7.90 eV) for the mass spectrometry, while the charged metal−silicon clusters were directly accelerated with a pulsed electric field. In all of the mass spectra, bimodal distributions were typically observed for $MSi_n^{-/0/+}$; the solid square (■) for $n = 6-11$ and the open circle (○) for $n = 12-20$ represent the two distributions (I and II).

In this modified cluster source, when the two plumes of the sample vapors were effectively mixed and reacted, the number of pure Si_n clusters was small, and the number of MSi_n clusters of interest was instead increased. When the vaporization laser for the metal rod was stopped, the pure Si_n clusters were enhanced without a significant formation of the binary M−Si clusters. This result shows that the MSi_n clusters were not formed by the laser vaporization of the metal-covered silicon rod, but by the mixing of two sample vapors with every shot.

As determined by an examination of the clusters' adsorption reactivities (described in section 3.2), the bimodal distributions correspond to the structural transition from metal-attached to metal-encapsulated structures. Distribution I, $n = 6-11$, was similar to that of pure Si_n, while distribution II, $n = 12-20$, exhibited a prominent peak at $MSi_{16}^{-/0/+}$. Within the pure Si_n clusters taken as a whole, the abundance of smaller Si_n clusters ($n = 6-11$) is relatively rich,[11,12] while larger sized Si_n clusters ($n \geq 12$) are relatively scarce. The similarity in $n = 6-11$ between Si_n and MSi_n was presumed to be due to the stability of the pure Si_n clusters and indicated that the MSi_n clusters ($n = 6-11$, distribution I) take a metal-atom "attached" structure, where the metal atom is located on the surface of the Si_n clusters.

Distribution II was, on the other hand, completely different from that of pure Si_n clusters, which exhibit a much lower abundance. In this distribution, as shown in Figures 2a−c, the selective formation of (a) $ScSi_{16}^-$, (b) $TiSi_{16}$, and (c) VSi_{16}^+ as "magic numbers" was found as a result of the different charge states of the anion, neutral, and cation, respectively.[18d] High intensities around MSi_{16} with various M atoms were similarly observed in the mass spectra of the MSi_n that had been mixed with one metal atom from the fourth period of Zr (e) and Nb (f) for the neutrals and from the fifth period of Hf (h) and Ta (i) for the cations. In particular, the doping of the transition metal atoms of Sc, Ti, V, Zr, Nb, Hf, and Ta provided the magic-number behavior of MSi_{16}, while the intensities of YSi_{16} and $LuSi_{16}$ were less prominent than that of the neighbors of $n = 15$ and 17, even for their anions.

To obtain magic clusters of MSi_n selectively at $n = 16$, the substitution of a Ti atom for a neighboring Sc or V requires a change in the total charge of the cluster. These three magic numbers of $ScSi_{16}^-$, $TiSi_{16}$, and VSi_{16}^+ demonstrate that the

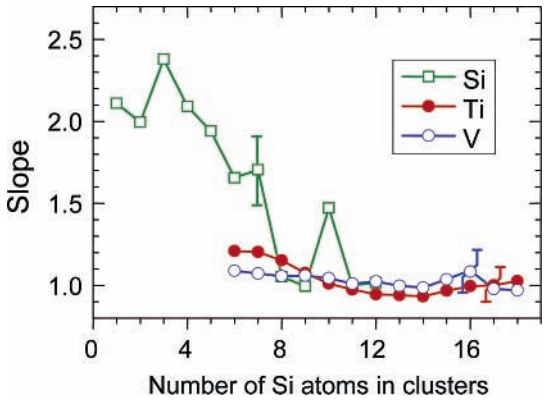

Figure 3. Slope of laser power dependence for the production of pure Si_n ($n = 1-12$) and MSi_n (M = Ti (●) and V (○); $n = 6-18$) with the F_2 laser. Although the slope is significantly above 1.0 for smaller cluster sizes, it becomes almost 1.0 within experimental uncertainties for the cluster sizes ($n = 12-18$) in the distribution II. Typical experimental uncertainties are shown.

$MSi_{16}^{-/0/+}$ clusters exhibit a closed electron configuration with the valence electrons of Sc^-, Ti, and V^+. The most plausible explanation is that the $TiSi_{16}$ assumes a closed electron configuration with tetravalent Ti and completes the electron shell to give either (1) 20 electrons with an electron in the $3p_z$ orbital of the sp^2-hybridized Si atoms or (2) 68 electrons with tetravalent Si atoms. Interestingly, either number of electrons satisfies the electronic shell closings predicted by the jellium model,[1] although this conjecture should be tested by theoretical calculations. Very recently, the stability of the $MSi_{16}^{-/0/+}$ clusters has been discussed by theoretical calculations.[27] Reveles and Khanna[27a] have proposed electron-counting rules based on the bond critical points, showing that the total number of 20 valence electrons contributes to the stability together with geometrical shapes.

It should be emphasized that the improvement consisting of face-to-face laser vaporizations of two rods accelerated the mixing of the two elements significantly. This magic-numbers behavior became much less prominent in other charged states; in Sc−Si compounds, for example, the magic number MSi_{16} appears only in the anions. As a neutral species, $TiSi_{16}$ could be formed, and as cationic species, VSi_{16}^+, $NbSi_{16}^+$, and $TaSi_{16}^+$ could be produced selectively by fine-tuning the source conditions, laser fluences, and flow rate of the He carrier. These magic-numbered clusters of MSi_{16} appeared to have a different geometric structure from that of the MSi_n in distribution I, and also, an electronic stabilization might have occurred. That is, one metal atom was seemingly encapsulated by the Si_n cluster cages to generate both an electronic and a geometric closure; this possibility is clearly indicated by adsorption reactivity and anion photoelectron spectroscopy results described below.

Note that in the photoionization of the MSi_n neutrals, the laser power dependence indicates that, for $n = 5-18$, one-photon ionization occurs not with the ArF laser (6.43 eV), but with the F_2 laser (7.90 eV). Figure 3 shows the slopes of laser power dependencies for pure Si_n (n = 1−12) and MSi_n (M = Ti and V, $n = 6-18$) with the F_2 laser. Although the slope is significantly above 1.0 for smaller cluster sizes of pure Si_n, it becomes almost 1.0, within experimental uncertainties, for the cluster sizes in distribution II, a result showing that the photoionization with the F_2 laser takes place in a one-photon process. In the photoionization mass spectra for the neutral species, dissociation might accompany photoionization when quite unstable cations are generated in the vertical photoionization process. Indeed, the geometric stability attributed to the

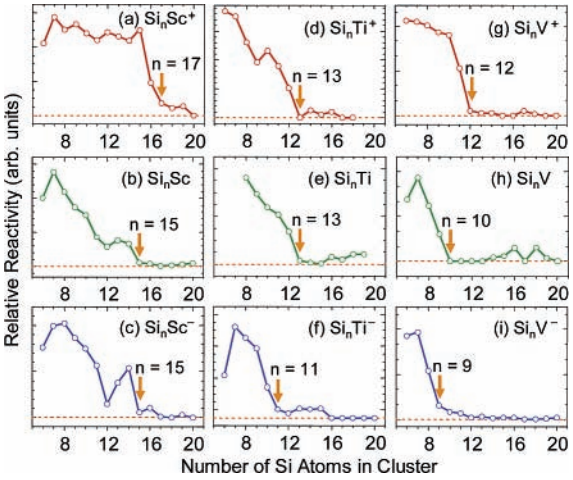

Figure 4. Relative reactivity of cationic/neutral/anionic $MSi_n^{-/0/+}$ toward H_2O vapor; (a)−(c) $ScSi_n^{-/0/+}$, (d)−(f) $TiSi_n^{-/0/+}$, and (g)−(i) $VSi_n^{-/0/+}$. Vertical arrows show the threshold size where the relative reactivity is lost. The threshold size for the metal atoms in group 3 is minimum of $n = 9$ for VS_n^-, whereas it is maximum of $n = 17$ for $ScSi_n^+$. The change in the threshold size can be reasonably explained by metal encapsulation in a Si cage.

highly symmetric structures of the MSi_{16} might be a major product of the dissociative photoionization, especially when the clusters are generated in hot conditions. However, the prominent magic-number behavior of MSi_{16} (M = Ti, Zr, and Hf) was instead emphasized when a colder condition was used with the high-pressure pulsed valve for expansion. This result shows that the relatively remarkable character of the photoionized MSi_{16}^+ can be ascribed to the rich abundance of the neutral form.

3.2. Adsorption Reactivity of MSi_n Clusters. *3.2.1. Metal Encapsulation.* To investigate the structure of MSi_n clusters, the cluster size dependence of the adsorption reactivity toward H_2O vapor was measured.[23] As reported previously,[18c,d] such a chemical probe method is useful in deducing the structure of the MSi_n clusters. Since the reactivity of Si_n is generally much lower than that of a metal atom, the reactivity is sensitive to location of the metal atom; high and low reactivities correspond to an exterior and an interior metal atom, respectively. Namely, it is expected that metal-encapsulated MSi_n shows no reactivity, and the threshold cluster size for the reactivity of MSi_n is indicative of the structural change to the metal encapsulation.

Figure 4 shows plots of the reactivity of MSi_n clusters (M = Sc, Ti, and V) in cationic, neutral, and anionic states toward H_2O vapors. Although the scale of the relative reactivity was varied within a factor of 2 by the kind of a metal atom and by the charge states, the reactivity generally decreases with an increasing number of Si atoms, and a "threshold size" of the reactivity is found where the reactivity is lost. The threshold sizes are summarized in Table 1, including those in the fourth and fifth period metal-atom-doped Si_n (see Figure 5). Note that the richly abundant species of $ScSi_{16}^-$, $TiSi_{16}$, VSi_{16}^+, $ZrSi_{16}$, $NbSi_{16}^+$, $HfSi_{16}$, and $TaSi_{16}^+$ seen in Figure 2 all exhibit no adsorption reactivity. Such a lack of reactivity can be reasonably ascribed to the metal-atom encapsulation in these magic-numbered clusters; otherwise, the metal atom would work as a reactive site. Indeed, the reactivity is recovered with the doping of the second metal atom, which appears on the surface of the cluster.

Figure 5 shows plots of the reactivity of cationic/neutral/anionic $M_{1,2}Si_n^{-/0/+}$ (M = Sc, Y, Lu, Ti, Zr, Hf, V, Nb, and Ta) toward H_2O vapor. Similarly to the results shown in Figure 4, the reactivity generally decreases with an increasing number

TABLE 1: Threshold Sizes of Adsorption Reactivity for Cationic/Neutral/Anionic MSi_n Clusters: (a) $ScSi_n$, (b) $TiSi_n$, (c) VSi_n, (d) YSi_n, (e) $ZrSi_n$, (f) $NbSi_n$, (g) $LuSi_n$, (h) $HfSi_n$, and (i) $TaSi_n$

	group 3			group 4			group 5		
	cation	neutral	anion	cation	neutral	anion	cation	neutral	anion
3d	(a) Sc: 1.63			(b) Ti: 1.45			(c) V: 1.31		
	17	15	15	13	13	11	12	10	9
4d	(d) Y: 1.78			(e) Zr: 1.59			(f) Nb: 1.43		
	21	20	20	15	14	12	13	12	11
5d	(g) Lu: 1.72			(h) Hf: 1.56			(i) Ta: 1.43		
	21	16	18	14	14	12	13	10	11

[a] A metallic bond radius was also listed, taken from ref 28.

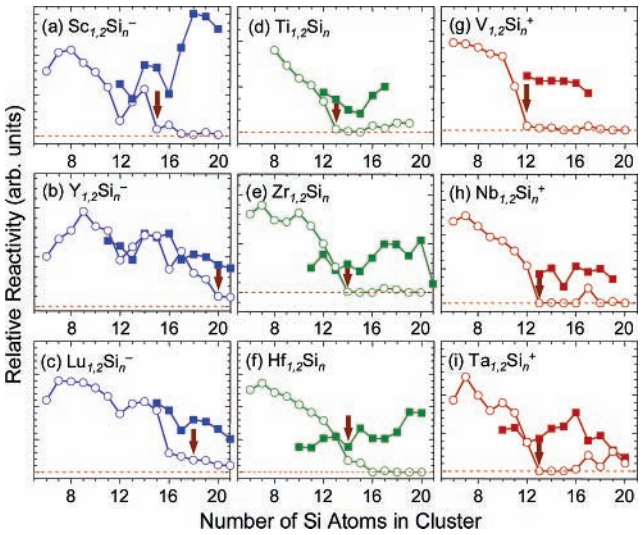

Figure 5. Relative reactivity of cationic/neutral/anionic $M_{1,2}Si_n^{-/0/+}$ toward H_2O vapor ($M_1Si_n^{-/0/+}$ (open circle: ○) and $M_2Si_n^{-/0/+}$(solid square: ■): (a) $Sc_{1,2}Si_n^-$, (b) $Y_{1,2}Si_n^-$, (c) $Lu_{1,2}Si_n^-$, (d) $Ti_{1,2}Si_n$, (e) $Zr_{1,2}Si_n$, (f) $Hf_{1,2}Si_n$, (g) $V_{1,2}Si_n^+$, (h) $Nb_{1,2}Si_n^+$, and (i) $Ta_{1,2}Si_n^+$. Vertical arrows show the threshold size of $M_1Si_n^{-/0/+}$ where the relative reactivity is lost. The threshold size for the metal atoms of Y and Lu is above $n = 16$, indicating that Y and Lu atoms are too large to be encapsulated by 16 Si atoms. The change in the threshold size can be reasonably explained by metal encapsulation in a Si cage.

of Si atoms, and a "threshold size" of the reactivity is found where the reactivity is lost. Above the threshold size, a metal atom is likely to be encapsulated within a Si cage because the reactivity is recovered with the doping of the second metal atom, which appears on the surface of the cluster. Very recently, photodissociation processes have been investigated for metal−silicon cluster cations,[18f] showing that the dissociation of $CrSi_{15}^+$ and $CrSi_{16}^+$ is definitely different from those of the smaller clusters, with elimination of silicon rather than metal. The photodissociation result implies encapsulated metal structures, which is consistent with this adsorption reactivity data.

Moreover, the following two points concerning the threshold sizes are apparent from Figure 4 and Table 1: (i) a charge state dependence and (ii) an element dependence within the same period. As for the charge state dependence, the threshold sizes decrease in the order of cation, neutral, and anion, when they are compared in Figure 4, parts a−c, d−f, and g−i, although the charge state dependence of anionic MSi_n^- (M = Lu and Ta) was exceptional. Within the same group with the same charge state, the threshold sizes of MSi_n clusters decrease with increasing atomic number, as in the comparisons seen in Figure 4: parts a, d, g; b, e, h; c, f, i. Furthermore, as tabulated in Table 1, the threshold sizes of MSi_n clusters for metals in the same group decrease in a similar manner with an increasing atomic number, as seen in Table 1: a−c, d−f, and g−i.

Both of the threshold size dependencies on charge state and element can be rationalized by metal encapsulation. When the radii of the metals of groups 3, 4, and 5 are compared (see Table 1 [ref 28]), the metallic radius generally decreases with increasing atomic number in the same period, while it increases with increasing atomic number in the same group. Since the threshold size decreases with smaller metal atoms, the threshold size indicates the number of silicon atoms required for the metal encapsulation. This result reveals that the enlargement of the silicon clusters rather takes place in the anions. Namely, the threshold size shows a minimum at a smaller metal atom in the MSi_n^- anions, whereas it has a maximum at the larger metal atom in the MSi_n^+ cations.

According to the ion mobility experiments on pure silicon clusters,[29] the anions have systematically longer drift times, and hence smaller mobilities, than the cations; the anions are effectively larger than the cations. This systematic shift was assigned not to a structural change, but to the extra charge causing the surface electron density of the anions to spill out further than for the cations.

When a metal atom is encapsulated inside a Si cage, the valence orbitals are significantly perturbed by the metal atoms and the extra electrons go into orbitals which lead to a substantial change in the framework of a silicon cage, the enlargement of the silicon cage seen in the anions. As indicated in Figure 4, in fact, the threshold size for the metal atoms in group 3 is minimum for $n = 9$ for VSi_n^-, whereas it is maximum for $n = 17$ for $ScSi_n^+$. As tabulated in Table 1, moreover, the threshold size shows a maximum at $n = 21$ for YSi_n^+ and $LuSi_n^+$.

It should be noted that a charge state dependence of the reaction products was observed. The products of the cationic MSi_n^+ in most of the reactions with H_2O were the H_2O adducts of $MSi_n{\cdot}H_2O$. However, the products of anionic Si_nTi^- and Si_nV^- were oxygen-atom adducts of $MSi_n{\cdot}O^-$. In the case of neutrals, furthermore, both $MSi_n{\cdot}H_2O$ and $MSi_n{\cdot}O$ adducts coexisted as reaction products. The change in the reaction products from $MSi_n{\cdot}H_2O^{+/0}$ to $MSi_n{\cdot}O^{0/-}$ indicates that an electron transfer takes place from MSi_n to H_2O because an electron occupation of an antibonding orbital of H_2O is likely to cause O−H bond dissociation. In fact, it seems that an electron transfer to H_2O occurs more extensively for the anionic clusters than for the cationic clusters, in the cases where the anionic clusters have two more electrons than the cations.

3.2.2. Cavity Size of a Si_{16} Cage. As discussed above in section 3.2.1, there exists a suitable cavity size in which the metal atom can be encapsulated by the Si_n cage. Here, the cavity size of a Si_{16} cage will be discussed. For the size of a metal atom, a metallic bond radius, rather than an ionic bond radius, is used as an index. According to several theoretical calculations on MSi_n (M = Ta, Ni, Re, and Zr),[30] charge transfer takes place from the silicon atoms to a metal atom at a larger size (above $n = 8-10$), especially when the metal atom is encapsulated,

and is generally negatively charged. As indicated by several theoretical calculations, the interaction between the metal atom and the Si_n is not of an ionic nature. Indeed, the theoretical result for metal-atom-encapsulated $TiSi_{16}$ suggests that the radius of the Ti atom is 1.47 Å,[19a] which is very close to the metallic radius of 1.45 Å.

However, the cavity size of a Si_{16} cage should be discussed for each polarity because the size of a Si_n cage apparently depends on the charge state of the MSi_n. As shown in Table 1, for an anionic Si_{16} cage, the threshold sizes of YSi_n^- and $LuSi_n^-$ were 20 and 18, respectively, and YSi_{16}^- and $LuSi_{16}^-$ still exhibited reactivity. Thus, a Y or Lu atom is too large to be encapsulated by the anionic Si_{16} cage. The threshold size of $ScSi_n^-$, on the other hand, is $n = 15$, and no reactivity is shown at $ScSi_{16}^-$. These results were apparently caused by the difference between the radii of the doped metal atoms. Since the metallic bond radii of Y and Lu are 1.78 and 1.72 Å, values which are much larger than that of Sc (1.63 Å), the cavity size can be deduced from these metal atom radii. Based on those for the metal-encapsulated $ScSi_{16}^-$ (Sc: 1.63 Å) and the nonencapsulated $LuSi_{16}^-$ (Lu: 1.72 Å), the cavity size of the anionic Si_{16} cage can be estimated to be between 3.26 and 3.44 Å in diameter. In the case of the neutral MSi_n clusters, the element dependence for the threshold size is almost the same as that for the anionic clusters. Thus, the cavity size of the neutral Si_{16} cage can also be estimated to be between 3.26 and 3.44 Å in diameter.

In the case of cationic MSi_n^+ clusters, all of the MSi_{16}^+ clusters containing groups 4 and 5 metal M atoms exhibited no reactivity, implying that the cationic Si_{16} cage has a sufficiently large inner cavity to encapsulate those metal atoms. Since a Zr atom has the largest atomic radius (1.59 Å) among the groups 4 and 5 metal atoms, the lower limit of the cavity size of the cationic Si_{16} cage must be 3.18 Å in diameter. For group 3 metal atoms, the threshold sizes are more than $n = 16$, and MSi_{16}^+ exhibited more or less reactivity. Since a Sc atom has the smallest radius of 1.63 Å, the cavity size for a cationic Si_{16} cage is between 3.18 and 3.26 Å in diameter. Hereafter, metal-atom-encapsulated Si_{16} clusters are expressed as $M@Si_{16}$.

It should be noted that for a rare-earth metal atom, the adsorption reactivity shows local minima at $n = 12$ and 16, although some reactivity was still apparent until $n = 18$ or 20. Since the enhanced formation of $LnSi_{12}$ and $LnSi_{16}$ was also observed in the mass spectra, these clusters might be somewhat stable electronically or geometrically, although the results indicate that the Ln atom might not be encapsulated completely at $n = 12$ and 16. Some theoretical results actually predict that such clusters could adopt a symmetrical structure: a Si_{12} hexagonal prism cage.[19]

3.3. Electronic Structure of MSi_{16}. To reveal the electronic stability of MSi_{16} clusters, the photoelectron spectra (PES) for the anionic clusters of MSi_{16}^- (M = Sc, Ti, V, Y, Zr, Nb, Lu, Hf, and Ta) were measured at 213 nm (5.83 eV). The spectral features, shown in Figure 6, of MSi_{16}^- doped with group 4 elements of Ti (d), Zr (e), and Hf (f) show a small bump around 2.8−3.0 eV (labeled X) in common, followed by a large energy gap and more discrete transitions at higher binding energies (A, B). Each spectrum yielded a vertical detachment energy (VDE) and an adiabatic detachment energy. The latter is the electron affinity (EA) of the cluster. These features are very different from those of the group 3 elements of Sc (a), Y (b), and Lu (c), and those for group 5 elements of V (g), Nb (h), and Ta (i), in which the detachment peaks start in the higher energy region above 3 eV without a separate peak like the peak X seen in

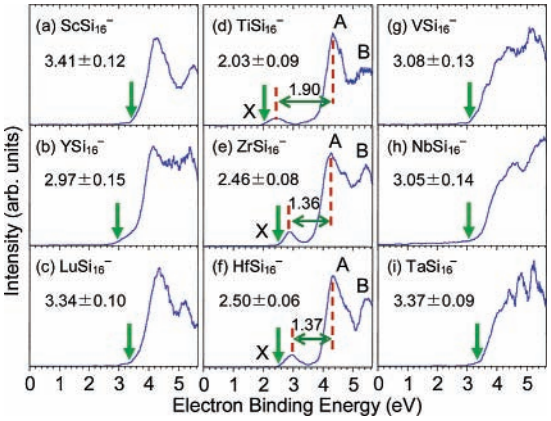

Figure 6. Photoelectron spectra of (a) $ScSi_{16}^-$, (b) YSi_{16}^-, (c) $LuSi_{16}^-$, (d) $TiSi_{16}^-$, (e) $ZrSi_{16}^-$, (f) $HfSi_{16}^-$, (g) VSi_{16}^-, (h) $NbSi_{16}^-$, and (i) $TaSi_{16}^-$ at 213 nm. Among them, the HOMO−LUMO gap energies for the spectra of (d) $TiSi_{16}^-$, (e) $ZrSi_{16}^-$, and (f) $HfSi_{16}^-$ are shown, indicating that $TiSi_{16}$ was the most stable among Ti (atomic radii: 1.45 Å), Zr (1.59 Å), and Hf (1.56 Å), and implying that the cluster anions have an excess electron in a singly occupied MO. Vertical arrows show an adiabatic detachment energy, of which the values are shown in eV.

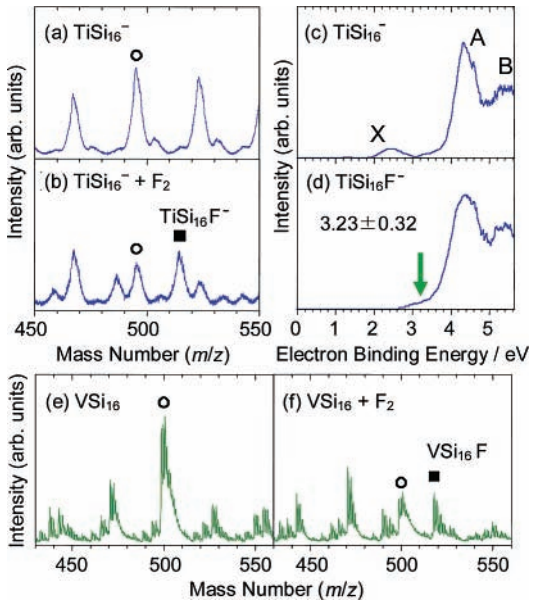

Figure 7. (a) and (b) show the mass spectra of $TiSi_{16}^-$ anions before and after reaction toward F_2, while (c) and (d) show the PES spectra of $TiSi_{16}^-$ and $TiSi_{16}F^-$ and (e) and (f) show the mass spectra of VSi_{16} neutral before and after the reaction. Open circles (○) and solid squares (■) represent the peaks of $TiSi_{16}^-$ anions or VSi_{16} neutrals, and $TiSi_{16}F^-$ anions or $VSi_{16}F$ neutrals. MSi_{16} clusters were converted to the ionic product of $MSi_{16}F$ in each mass spectrum ((a), (b), (e), and (f)). The small peak (X) around 2.5 eV in the PES spectrum of (c) $TiSi_{16}^-$ disappeared in that of (d) $TiSi_{16}F^-$ after the reaction. These results indicate the formation of an ionically bound superatom complex.

$TiSi_{16}^-$. If peak X in the PES spectrum of $Ti@Si_{16}^-$ truly corresponds to a singly occupied MO (SOMO), this spectral pattern suggests that $Ti@Si_{16}$ neutral is a closed-shell molecule with a large HOMO−LUMO gap. Experimental verification of single occupation was achieved by our established technique of halogen atom doping.[31] Briefly, for the nondegenerate SOMO in geometrically rigid clusters, a halogen atom can remove the single electron from the SOMO without any serious distortions.

Figure 7 shows the mass spectra for the formation of fluorine (F) atom adducts of $TiSi_n^-$ anions ($n = 15$−17), before and after the adsorption reaction of F_2. Although the $TiSi_{16}$ neutral is nonreactive toward F_2, $Ti@Si_{16}^-$ is reactive, forming the

F-atoms adduct $Ti@Si_{16}Fi^-$. Furthermore, in the 213-nm spectrum of $Ti@Si_{16}Fi^-$ shown in Figure 7d the peak X disappears, while the other spectral features seen in the unreacted spectrum of Figure 7c are maintained. Since feature A corresponds to the lowest triplet state of the neutral compound, the A−X separation, measured to be 1.90 eV, represents the excitation energy of the first triplet states of neutral $Ti@Si_{16}$, which is also an approximate experimental measure of the HOMO−LUMO gap. Interestingly, the spectral features of $Ti@Si_{16}F^-$ roughly resemble those of $Sc@Si_{16}^-$, which is consistent with them both having an isoelectronic framework of $M@Si_{16}$. What is surprising is the magnitude of the HOMO−LUMO gap: that observed for $TiSi_{16}$ is the largest among those measured for single metal atom doped silicon clusters. It is very comparable with that observed in the recently discovered 20-electron tetrahedral Au_{20} cluster.[7]

As shown in Figures 6d−f, the large HOMO−LUMO gaps of $Ti@Si_{16}$, $Zr@Si_{16}$, and $Hf@Si_{16}$ were found to be 1.90, 1.36, and 1.37 eV, respectively. The order of these values is consistent with that of the atomic radii of these metal atoms, which are 1.45, 1.59, and 1.56 Å, respectively. Since the atomic radius of Hf is smaller than that of Zr, neutral $Hf@Si_{16}$ is somewhat more stable than $Zr@Si_{16}$, and the smallest Ti atom results in the largest HOMO−LUMO gap of these $M@Si_{16}$ compounds. The largest HOMO−LUMO gap of $TiSi_{16}$ suggests that it should be very inert and may possess a highly symmetrical geometry; the radii of Zr and Hf atoms make them likely to be somewhat too large to be encapsulated by a 16 Si-atom cage. A correlation between energy gaps and stability is generally found for metal clusters,[32] where the magic numbers of particularly stable clusters are associated with the existence of a HOMO−LUMO gap. With isoelectronic dopings of Ti, Zr, and Hf atoms, the HOMO−LUMO gap correlates closely with geometric stability. In fact, it has been proposed that $Ti@Si_{16}$ assumes the metal-encapsulated structure of a Frank-Kasper polyhedron,[33] calculated to have an EA of 1.90 eV and a HOMO−LUMO gap of 2.35 eV.[19a,b]

Several theoretical calculations on the bond formation between Si_n and M and the nature of their orbitals have been reported. In the calculation for $ReSi_{12}$,[30c] the electron configuration on the Re atom is $(6s)^{0.44}(5d)^{7.67}(6p)^{0.17}(7s)^{0.02}(6d)^{0.05}$, quite different from the ground state of Re of $(6s)^2(5d)$.[5] The decrease in the number of 6s electrons, while the number of 5d electrons increases, indicates hybridization of 5d and 6s orbitals.

Froudakis and co-workers have found that the character of the HOMO and LUMO of early transition metal (V) atom doped VSi_n is dominated by both the d orbitals of V and the s−p orbitals of Si.[34] The contribution of d orbitals in the HOMO and LUMO of MSi_n causes a negative population of electrons on the metal atom, implying that the metal d orbitals stabilize the spherical structure of the sp^2-hybridized Si cage to form the metal encapsulation of MSi_{16}. Similar cooperative stabilization between metal d orbitals and a sp^2-hybridized cage has been reported theoretically for a metal-encapsulated carbon cage, $M@C_{28}$,[35] where the d orbital of a Zr atom can electronically contribute to encouraging the encapsulation in a carbon cage. From a geometric point of view, however, the striking contrast between $M@Si_n$ and $M@C_n$ is packing density; in $M@Si_{16}$, a metal atom is tightly trapped within the Si atoms, while in $M@C_n$ some space is left for the metal atom to move around inside the carbon cage.

3.4. Reaction of $TiSi_{16}^-$ and VSi_{16} toward F_2. A "magic" cluster of a metal atom encapsulated in a Si cage can be viewed as a superatom. The $Ti@Si_{16}$, $Zr@Si_{16}$, and $Hf@Si_{16}$ clusters of binary M−Si can be viewed as rare-gas-like superatoms, while $Sc@Si_{16}$ and $M^V@Si_{16}$ (M^V = V, Nb, and Ta) can be viewed as halogen-like and alkali-like superatoms, respectively. As shown in Figure 7b, $Ti@Si_{16}^-$, which has an excess electron, was converted to the product of $Ti@Si_{16}F^-$ because the excess electron of $Ti@Si_{16}^-$ is quenched by a halogen F atom. Moreover, by careful adjustment of the flow of F_2, $V@Si_{16}$ could be converted into $V@Si_{16}F$ (Figures 7e,f). It should be noted that the $V@Si_{16}^+$ cation is nonreactive toward F_2, as is the $Ti@Si_{16}$ neutral. The halogen atom addition reaction of $V@Si_{16}$ shows that this cluster is an alkali atom-like species, and that $V@Si_{16}F$ is an ionically bound superatom complex, whereas $V@Si_{16}^+$, having a structure isoelectronic with $Ti@Si_{16}$, is electronically closed.

The photoelectron spectra of $Sc@Si_{16}^-$ yielded a VDE of 4.25 eV and an adiabatic detachment energy of 3.41 eV, values much larger than those of other metal-doped silicon clusters. This pronounced stability of $Sc@Si_{16}^-$ is very similar to that of Al_{13}^-,[36] where Al_{13} can be viewed as a superhalogen having high EA.[37] Current studies involving the reaction of metal atom encapsulated silicon cages with halogen atoms imply that it may be possible to form "cluster-salt crystals" as well as the theoretically predicted superatom salt of $Al_{13}K$.[38]

4. Conclusions

The transition metal doped silicon clusters, MSi_n, were generated by the laser vaporization method in a modified cluster source, and their stability was characterized with mass distribution, adsorption reactivity, and PES. With a systematic doping of transition metal atoms of groups 3, 4, and 5 (M = Sc, Y, Lu, Ti, Zr, Hf, V, Nb, and Ta) together with variations in the charge states, we found that anionic $Sc@Si_{16}^-$, neutral $Ti@Si_{16}$, and cationic $V@Si_{16}^+$, $Nb@Si_{16}^+$, and $Ta@Si_{16}^+$ were generated in large quantities due to both electronic and geometric closings. These magic-numbered $M@Si_{16}^{-/0/+}$ clusters have 20 (68) valence electrons in common. The charge state dependence of relative reactivity also implies an enlargement of Si_n cage with increasing numbers of valence electrons. The element dependencies revealed that the critical size of the Si_{16} cage cavity for metal encapsulation is 3.2−3.4 Å in diameter. Anion photoelectron spectroscopy has revealed that the small atomic radius of Ti results in $Ti@Si_{16}$ having the largest HOMO−LUMO gap of 1.90 eV among $Ti@Si_{16}$, $Zr@Si_{16}$, and $Hf@Si_{16}$. The most suitable metals for encapsulation were Ti, found in $Ti@Si_{16}$ neutrals, and V, Nb, and Ta, found in the cations of $V@Si_{16}^+$, $Nb@Si_{16}^+$, and $Ta@Si_{16}^+$. Combined with the known superhalogen Al_{13}, the existence of the silicon-based superatom family of $Sc@Si_{16}^-$, $Ti@Si_{16}$, $V@Si_{16}^+$, $Nb@Si_{16}^+$, and $Ta@Si_{16}^+$ suggests that it should be possible to create Si-based cluster-assembled materials.

Acknowledgment. This work is partly supported by the Ministry of Education, Culture, Sports, Science and Technology (MEXT), Grant-in-Aid for the 21st Century COE program "KEIO LCC". K.K. is grateful for Research Fellowship of the JSPS for Young Scientists.

References and Notes

(1) Knight, W. D.; Clemenger, K.; de Heer, W. A.; Saunders, W. A.; Chou, M. Y.; Cohen, M. L. *Phys. Rev. Lett.* **1984**, *52*, 2141.

(2) Kappes, M. M.; Kunz, R.; Schumacher, E. *Chem. Phys. Lett.* **1985**, *119*, 11.

(3) Iniguez, M. P.; Alonso, J. A.; Rubio, A.; Lopez, M. J.; Balbas, L. C. *Phys. Rev. B* **1990**, *41*, 5595.

(4) Kroto, H. W.; Heath, J. R.; O'Brien, S. C.; Curl, R. F.; Smalley, R. E. *Nature* **1985**, *318*, 162.
(5) Takata, M.; Umeda, B.; Nishibori, E.; Sakata, M.; Saitoh, Y.; Ohno, M.; Shinohara, H. *Nature* **1995**, *377*, 46.
(6) Guo, B. C.; Kerns, K. P.; Castleman, A. W., Jr. *Science* **1992**, *255*, 1411.
(7) Li, J.; Li, X.; Zhai, H.-J.; Wang, L.-S. *Science* **2003**, *299*, 864.
(8) Pyykkö P.; Runeberg, N. *Angew. Chem., Int. Ed.* **2002**, *41*, 2174.
(9) Yeretzian, C.; Röthlisberger, U.; Schumacher, E. *Chem. Phys. Lett.* **1995**, *237*, 334.
(10) Nakajima, A.; Kaya, K. *J. Phys. Chem. A* **2000**, *104*, 176.
(11) Li, B.-X.; Cao, P.-L. *Phys. Rev. A* **2000**, *62*, 023201, and references therein.
(12) Jarrold, M. F.; Bower, J. E. *J. Chem. Phys.* **1992**, *96*, 9180.
(13) (a) Raghavachari, K.; Rohlfing, C. M. *J. Chem. Phys.* **1988**, *89*, 2219. (b) Raghavachari, K. *J. Chem. Phys.* **1986**, *84*, 5672.
(14) Röthlisberger, U.; Andreoni, W.; Parrinello, M. *Phys. Rev. Lett.* **1994**, *72*, 665.
(15) Menon, M.; Subbaswamy, K. R. *Chem. Phys. Lett.* **1994**, *219*, 219.
(16) Ho, K.-M.; Shvartsburg, A. A.; Pan, B.; Lu, Z.-Y.; Wang, C.-Z.; Wacker, J. G.; Fye, J. L.; Jarrold, M. F. *Nature* **1998**, *392*, 582.
(17) Rata, I.; Shvartsburg, A. A.; Horoi, M.; Frauenheim, T.; Siu, K. W. M.; Jackson, K. A. *Phys. Rev. Lett.* **2000**, *85*, 546.
(18) (a) Sanekata, M.; Koya, T.; Nagao, S.; Negishi, Y.; Nakajima, A.; Kaya, K. *Trans. Mater. Res. Soc. Jpn.* **2000**, *25*, 1003−1006. (b) Hiura, H.; Miyazaki, T.; Kanayama, T. *Phys. Rev. Lett.* **2001**, *86*, 1733−1736. (c) Ohara, M.; Koyasu, K.; Nakajima, A.; Kaya, K. *Chem. Phys. Lett.* **2003**, *371*, 490−497. (d) Koyasu, K.; Akutsu, M.; Mitsui, M.; Nakajima, A. *J. Am. Chem. Soc.* **2005**, *127*, 4998. (e) Zheng, W.; Nilles, J. M.; Radisic, D.; Bowen, K. H., Jr. *J. Chem. Phys.* **2005**, *122*, 071101. (f) Jaeger, J. B.; Jaeger, T. D.; Duncan, M. A. *J. Phys. Chem. A* **2006**, *110*, 9310.
(19) (a) Kumar, V.; Kawazoe, Y. *Phys. Rev. Lett.* **2001**, *87*, 045503. (b) Kumar, V.; Kawazoe, Y. *Phys. Rev. B* **2003**, *68*, 155412. (c) Kawamura, H.; Kumar, V.; Kawazoe, Y. *Phys. Rev. B* **2005**, *71*, 075423. (d) Kumar, V.; Majumder, C.; Kawazoe, Y. *Chem. Phys. Lett.* **2002**, *363*, 319. (e) Kumar, V. *Eur. Phys. J. D* **2003**, *24*, 227. (f) Ma, L.; Zhao, J.; Wang, J.; Lu, Q.; Zhu, L.; Wang, G. *Chem. Phys. Lett.* **2005**, *411*, 279. (g) Sen, P.; Mitas, L. *Phys. Rev. B* **2003**, *68*, 155404. (h) Lu, J.; Nagase, S. *Phys. Rev. Lett.* **2003**, *90*, 115506. (i) Khanna, S. N.; Rao, B. K.; Jena, P. *Phys. Rev. Lett.* **2002**, *89*, 016803. (j) Hagelberg, F.; Xiao, C.; Lester, W. A., Jr. *Phys. Rev. B* **2003**, *67*, 035426. (k) Andriotis, A. N.; Mpourmpakis, G.; Froudakis, G. E.; Menon, M. *New J. Phys.* **2002**, *4*, 78.1−78.14.
(20) Beck, S. M. *J. Chem. Phys.* **1987**, *87*, 4233; **1989**, *90*, 6306−6312.
(21) Watanabe, H. *The Physics and Fabrication of Micro-structures*; Kelley M. J., Weisbuch, C., Eds.; Springer: Heidelberg, 1986; pp 158−171.
(22) Even, U.; Jortner,J.; Noy, D.; Lavie, N.; Cossart-Magos, C. *J. Chem. Phys.* **2000**, *112*, 8068.
(23) Geusic, M. E.; Morse, M. D.; O'Brien, S. C.; Smalley, R. E. *Rev. Sci. Instrum.* **1985**, *56*, 2123.
(24) Ho, J.; Kent, M.; Ervin, K. M.; Lineberger, W. C. *J. Chem. Phys.* **1990**, *93*, 6987.
(25) Moore, C. E. Atomic Energy Levels as Derived from the Analyses of Optical Spectra; NSRDS-NBS 35, vol. 3; U.S. National Bureau of Standards: Washington, DC, 1971.
(26) (a) Harris, T. J. *IBM J. Res. Develop.* **1963**, *7*, 342, (b) Geohegan, D. B. *Appl. Phys. Lett.* **1992**, *60*, 2732, (c) Geohegan, D. B. *Appl. Phys. Lett.* **1993**, *62*, 1463.
(27) (a) Reveles, J. U.; Khanna, S. N. *Phys. Rev. B* **2006**, *74*, 035435. (b) Chen, Z.; Neukermans, S.; Wang, X.; Janssens, E.; Zhou, Z.; Silverans, R. E.; King, R. B.; Schleyer, P. R.; Lievens P. *J. Am. Chem. Soc.* **2006**, *128*, 12829.
(28) (a) Emsley, J. *The Elements*; Oxford University Press: New York, 1989. (b) Lide, D. R. *CRC Handbook of chemistry and physics. 79th Edition*; CRC Press: Boca Raton, FL, 1999.
(29) Hudgins, R. R.; Imai, M.; Jarrold, M. F.; Dugourd, P. *J. Chem. Phys.* **1999**, *111*, 7865.
(30) (a) Guo, P.; Ren, Z.-Y.; Wang, F.; Bian, J.; Han, J.-G.; Wang, G.-H. *J. Chem. Phys.* **2004**, *121*, 12265. (b) Ren, Z.-Y.; Li, F.; Guo, P.; Han, J.-G. *J. Mol. Struct.: THEOCHEM* **2005**, *718*, 165. (c) Han, J.-G.; Ren, Z.-Y.; Lu, B.-Z. *J. Phys. Chem. A* **2004**, *108*, 5100. (d) Wang, J.; Han, J.-G. *J. Chem. Phys.* **2005**, *123*, 064306.
(31) Kawamata, H.; Negishi, Y.; Kishi, R.; Iwata, S.; Nakajima, A.; Kaya, K. *J. Chem. Phys.* **1996**, *105*, 5369.
(32) de Heer, W. A. *Rev. Mod. Phys.* **1993**, *65*, 611.
(33) Frank, F. C.; Kasper, J. S. *Acta Crystallogr.* **1958**, *11*, 184−190.
(34) Mpourmpakis, G.; Froudakis, G. E.; Andriotis, A. N.; Menon, M. *J. Chem. Phys.* **2003**, *119*, 7498.
(35) Jackson, K.; Kaxiras, E.; Pederson, M. R. *J. Phys. Chem.* **1994**, *98*, 7805.
(36) Gergeron, D. E.; Castleman, A. W., Jr.; Morisato, T.; Khanna, S. N. *Science* **2004**, *304*, 84−87.
(37) Gutsev, G. L.; Boldyrev, A. I. *Usp. Khim.* **1987**, *56*, 889−910.
(38) Khanna, S. N.; Jena, P. *Chem. Phys. Lett.* **1994**, *219*, 479−483.